Journal of the European Ceramic Society 42 (2022) 6192–6198

Contents lists available at ScienceDirect

Journal of the European Ceramic Society

journal homepage: www.elsevier.com/locate/jeurceramsoc

Engineering of silicone-based blends for the masked stereolithography of biosilicate/carbon composite scaffolds

Paulina Ożóg [a], Hamada Elsayed [b,c], Luca Grigolato [b,d], Gianpaolo Savio [d], Jozef Kraxner [a], Dušan Galusek [a,e], Enrico Bernardo [b,*]

[a] FunGlass – Centre for Functional and Surface Functionalized Glass, Alexander Dubcek University of Trenčín, Trenčín, Slovakia
[b] Department of Industrial Engineering, University of Padova, Padova, Italy
[c] Ceramics Department, National Research Centre, El-Bohous Street, Cairo 12622, Egypt
[d] Department of Civil, Environmental and Architectural Engineering: Dept. ICEA, University of Padova, Padova, Italy
[e] Joint Glass Centre of the IIC SAS, TnUAD and FChFT STU, Centre for Functional and Surface Functionalized Glass, TnUAD, Trenčín, Slovakia

ARTICLE INFO

Keywords:
Biosilicate® glass-ceramic
Polymer-derived-ceramics
SiOC
Additive manufacturing
Masked stereolithography

ABSTRACT

Silicone resins, filled with phosphates and other oxide fillers, have been recently proposed as feedstock for the manufacturing of scaffolds with a composition resembling that of commercial Biosilicate® glass-ceramics. Silicones and engineered fillers enable the preparation of novel carbon-containing Biosilicate-based composites and, fundamentally, the easy application of additive manufacturing technologies. After successful demonstration of the applicability of direct ink writing of silicone-based pastes, the present paper is dedicated to preparation of highly porous scaffolds obtained by masked stereolithography, starting from a simple blend of silicone resin with commercial photocurable acrylates. Deviations in the desired phase assemblage were corrected by calibration of the silicone/fillers ratio. The more advanced printing technology, combined with ceramic transformation, allowed fabrication of scaffolds with a complex geometry and a distinctive control of overall porosity.

1. Introduction

In the last decade, the use of silicone polymers as raw materials for silicate bioceramics has been documented by a number of investigations [1–6]. A key feature of the process is the high reactivity of the silica-based residue, resulting from the thermal decomposition of silicones, with nano- and micro-sized oxide inclusions. Such oxide inclusions typically derive from fillers, mostly added in the form of carbonates and hydroxides dispersed in the polymer matrix [7]. The reactivity, generally expressed in terms of low processing temperatures and high phase purity [7], is accompanied by the fundamental advantage of preceramic polymers, consisting of the feasibility of simple, widely available, cost-effective polymer shaping technologies on silicone-based components before heat treatment and ceramic transformation.

Hydrated borates and phosphates may be seen as multiform fillers, contributing to both shaping and synthesis. Since dehydration occurs at low temperatures (<350 °C), water vapor is released into silicones still in their polymer state, resulting in their foaming. Upon firing, borates and phosphates generate a liquid phase, catalyzing the ionic interdiffusion, and transforming into a glassy phase upon cooling. A proper calibration of the content of borate and phosphate fillers with respect to the content of silicone and other fillers yields a new kind of glass-ceramics, which is not the result of crystallization of a parent glass [8]. Despite of lack of any crystallization treatment the products may be classified as glass-ceramics because of their nearly perfect match in the final phase assemblage between polymer-derived materials and glass-ceramics from the thermal treatment of parent glasses with the same overall oxide composition [9].

Polymer shaping technologies include additive manufacturing. Silicone and fillers, combined with suitable amounts of solvents (e.g. isopropyl alcohol) can easily yield pseudo-plastic pastes that can be used for the direct ink writing of reticulated scaffolds with hierarchical porosity [8,9]. In printed structures, macro-sized pores from printing may be accompanied by micro-sized pores in the struts arising from the dehydration of hydrated borate and phosphate fillers at the early stages of heat treatment. Silicone and fillers, however, may be used also beyond direct ink writing, particularly for the development of much more complex scaffolds by stereolithography. In this field, the need for preceramic polymers functionalized with photosensitive groups,

* Corresponding author.
E-mail address: enrico.bernardo@unipd.it (E. Bernardo).

https://doi.org/10.1016/j.jeurceramsoc.2022.06.057
Received 14 April 2022; Received in revised form 17 June 2022; Accepted 18 June 2022
Available online 22 June 2022
0955-2219/© 2022 The Authors. Published by Elsevier Ltd. This is an open access article under the CC BY-NC-ND license (http://creativecommons.org/licenses/by-nc-nd/4.0/).

previously announced after a first series of studies [10,11], has been recently refuted. In fact, stereolithography may be applied to simple silicone-based blends, consisting of a silicone polymer (and fillers) mixed with photocurable acrylates [12–14].

Silicones offer an unprecedented opportunity for the direct synthesis of carbon-containing glass-ceramic nano-composites. When treated in non-oxidative atmosphere, silicones transform into SiOC (silicon oxy-carbide) nanocomposites, consisting of turbostratic carbon nano-sheets embedded in a C-modified silica glass matrix, featuring Si-C bonds in addition to Si-O bonds [15]. The reaction with oxide fillers allows for the development of silicates, such as larnite (Ca_2SiO_5) or forsterite (Mg_2SiO_5) obtained by Fu et al. [16] and Zhu et al. [17], respectively, mixed with pyrolytic carbon. The presence of carbon phase promotes osteogenic differentiation [18] and, above all, enhances absorption of infrared light. The overheating of C-containing scaffolds under infrared light can be utilized in cancer therapy or for disinfection [19–23]. Recent investigations confirmed the functionalization of polymer-derived materials resembling the well-established Biosilicate® glass-ceramics by the presence of pyrolytic carbon [24].

The present paper is dedicated to the optimization of polymer-derived glass-ceramics resembling the Biosilicate® glass-ceramics, manufactured in the form of highly porous scaffolds by masked stereo-lithography. In this technology, thin layers of photosensitive resin deposited on a FEP (fluorinated ethylene propylene) plastic film are selectively cured by light passing through an underneath LCD screen (Fig. 1). Light from LED array passes only through the white pixels on the display, curing the photosensitive material and defining a projection area for each printed layer [25]. We will show that the adopted silicone-based technology, with appropriate polymer/filler ratios, did not only optimize the phase assemblage, but also allowed for some compensation of coarsening effects arising from the printing operations, which complicate the control of overall porosity.

2. Experimental procedure

2.1. Starting materials

A commercial solid silicone resin, H44 (Wacker-Chemie GmbH, Munich, Germany) was considered as the silica precursor. The silicone was blended with a commercial photocurable liquid acrylate (acrylate monomers and glycol diacrylate monomers mixed with phosphine oxide-based photo initiator, SB, Fun To Do, Alkmaar, The Netherlands), with isopropyl alcohol (IPA) as a solvent. The mixture, in the weight proportion H44/SB/IPA= 1/1/0.5, was homogenized by a planetary mixer (Thinky Are-250, Intertronics, Kidlington, UK), at a speed of 2000 rpm for 30 min. Fillers were then added in the amounts specified in Table1, and subsequently homogenized in the planetary mixer for another 30 min. Calcium carbonate ($CaCO_3$, <10 μm, industrial grade, Bitossi, Vinci, Italy), sodium carbonate (Na_2CO_3, <10 μm, reagent grade, Sigma-Aldrich, Germany) and sodium phosphate ($Na_4P_2O_6$, <10 μm, reagent grade, Sigma-Aldrich, Germany) were used as the fillers. Additional experiments carried out with a lower content of the silicone resin, decreased by 13.5 (S-13) and 27 wt% (S-27).

2.2. Printing of scaffolds

A first step involved the definition of geometrical models as a polygonal mesh, i.e. a set of adjacent triangular faces describing the surface of the samples. Then, the mesh was exported in the STL file format (Standard Triangulation Language) consisting of a list of tri-angles, reporting for each one the vertices coordinates and the face normal. All the samples consisted of gyroids (Fig. 2), i.e. structures in which the porosity is not defined as the space between interconnected beams ('struts'), but it corresponds to variously packed helicoidal channels, divided by curved membranes. More precisely, gyroid is a kind of triply periodic minimal surface, defined as periodic surfaces along x, y and z axes, with zero mean curvature, usually described as an implicit

Table1
Reference batch formulations for polymer-derived biosilicate scaffolds.

Oxides in Biosilicate® [wt%]	Oxide quantities related to 1 g of SiO_2 in Biosilicate® [g]		Source quantities referred to 1 g of SiO_2 / source
SiO_2 [48.5]	1		2.6 / H44 2.25 / H44 (S-13) 1.9 / H44 (S-27)
CaO [23.75]	0.490		0.874 /$CaCO_3$
P_2O_5 [4]	0.083		0.165 / $Na_4P_2O_6$
Na_2O [23.75]	0.490	0.072	0.072 / $Na_4P_2O_6$
		0.418	0.714 / Na_2CO_3

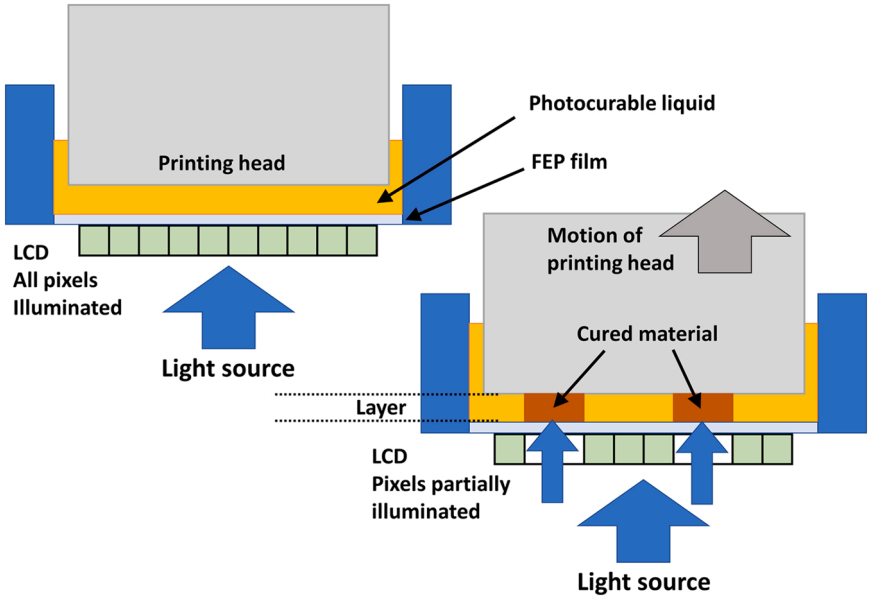

Fig. 1. Scheme of masked stereolithography 3D-printing.

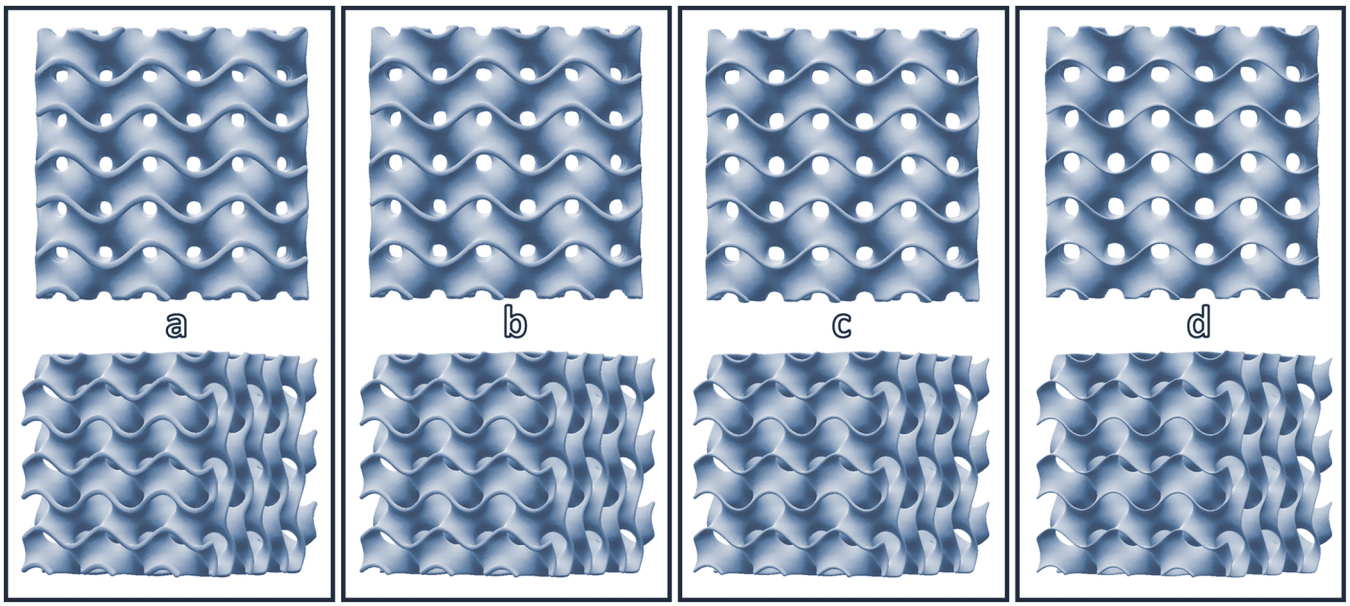

Fig. 2. Side (top) and perspective (bottom) views of gyroid scaffolds with increasing porosity: a) 75 vol%; b) 80%; c) 85%; d) 90%.

surface: (2πx/cs)*cos(2πy/cs)+sin(2πy/cs)*cos(2πz/cs)+sin(2πz/cs)cos(2πx/cs)= 0.

where cs is the cell size [26]. The overall porosity may be tuned according to the ratio between membrane thickness and channel size. Fig. 2 displays cubic blocks (15 mm × 15 mm × 15 mm), with a gyroid structure, having a different overall porosity, ranging from 75 to 90 vol %. They derived from a preliminary computational study by the Rhinoceros® 6 program package (Robert McNeel & Associates, Seattle, WA, USA), according to the approach described by Savio et al. [27], which is based on mesh modeling instead of implicit surface modeling. Successive studies show that the deviation from the implicit model and the mesh is lower than 1.1% of the cell dimension [28].

Three-dimensional scaffolds were manufactured with the use of a masked stereolitography printer (Original Prusa SL-1, Prusa Research a. s., Prague, Czech Republic) operating in the visible light range (405 nm). The layer thickness was set at 50 μm and the exposure time at 15 s. After printing, the structures were cleaned by compressed air and by washing in isopropyl alcohol. After further curing in a UV chamber (365 nm, Robotfactory S.r.l., Mirano, Italy), for 30 min, scaffolds were ceramized by a two-step heat treatment in flowing nitrogen (0.5 °C/min up to 500 °C for 5 h, followed by heating at 2 °C/min up to 1000 °C for 1 h).

2.3. Characterization of scaffolds

Density and porosity values were determined from geometrical measurements of regular blocks (geometrical density from the mass/volume ratio) and helium pycnometry (Micromeritics AccuPyc 1330, Norcross, GA), on whole scaffolds or on powdered materials, before and after heat treatment. Phase composition was evaluated by X-ray powder diffraction (XRD, Bruker AXS D8 Advance, Bruker, Germany), supported by the Match! program package (Crystal Impact GbR, Bonn, Germany). The microstructure was examined by scanning electron microscopy (SEM, FEI Quanta 200 ESEM, Eindhoven, Netherlands) equipped with energy dispersive X-ray spectroscopy (EDS). The crushing strength was measured on regular blocks (~10 mm × 10 mm × 10 mm, from the firing of regular printed blocks), using a universal materials testing machine (Quasar 25, Galdabini, Cardano, Italy), operating at a cross-head speed of 1 mm min^{-1}; each data point represents an average value obtained by testing at least eight specimens.

Fine Biosilicate® glass-ceramic powders (< 5 μm) (from controlled glass crystallization) were used as reference in terms of phase development and chemical composition. Specific surface area was determined by N_2 physisorption at − 196 °C (ASAP 2010, Micromeritics, Norcross GA, USA), by applying the Brunauer-Emmett-Teller (BET) multipoint method.

3. Results and discussion

After firing in N_2 at 1000 °C the resin was expected to yield a SiOC ceramic residue with the yield of 72% by weight related to weight of the resin. According to elemental analysis [29], the H44-derived ceramic residue is described by the formula $Si_3O_{4.6}C_{8.45}$, corresponding to a mixture of silica, carbon and SiC, as follows:

$$Si_3O_{4.6}C_{8.45} \leftrightarrow 2{\cdot}3\ SiO_2 + 0.7\ SiC + 7{\cdot}75C$$

The reference formulation, shown in Table1, was based on the assumption that only the silica fraction of the ceramic residue reacts with the oxide fillers. The other products (SiC and C) were considered inert, remaining in the system as extra phases. The fillers were expected to favor the phase separation which, in the residue from pure silicone resin, occurs typically above 1200 °C [15]. The ceramization of 26.2 g of H44 was expected to yield 18.9 g of ceramic residue corresponding to 10 g of SiO_2 and 8.9 g of other phases. Such assumption was supported by the results of direct foaming and direct ink writing experiments, showing the presence of graphene-like carbon, likely coupled with SiC nanocrystals [9]. These phases accompanied the main phase of sodium calcium silicate ($Na_2CaSi_2O_6$), matching the phase found in Biosilicate® glass-ceramics.

Preliminary stereolithography studies using the formulations from Table1 were not successful, and $Na_2CaSi_2O_6$ was accompanied by additional phases: along with the traces of ($NaCaPO_4$), found also in Biosilicate® glass-ceramics [14], a second Na-Ca silicate crystalline phase ($Na_2Ca_3Si_6O_{16}$) was also detected in a first series of scaffolds (formulation 'S' in Fig. 3a).

In the attempt to 'force' the separation of the ceramic residue into reactive silica and carbon-containing phases, the amount of silicone in the blends was progressively reduced, by 13.5 and 27 wt%. The second reduction made the silicone/fillers balance identical to the one used for H44-derived foams [24] fired in air, when H44 transforms into pure silica. As shown in Fig. 3a, the reduction of the silicone content had a positive impact on the phase composition. Diffraction maxima attributed to the silicate phase $Na_2Ca_3Si_6O_{16}$ were still visible with the 13.5%

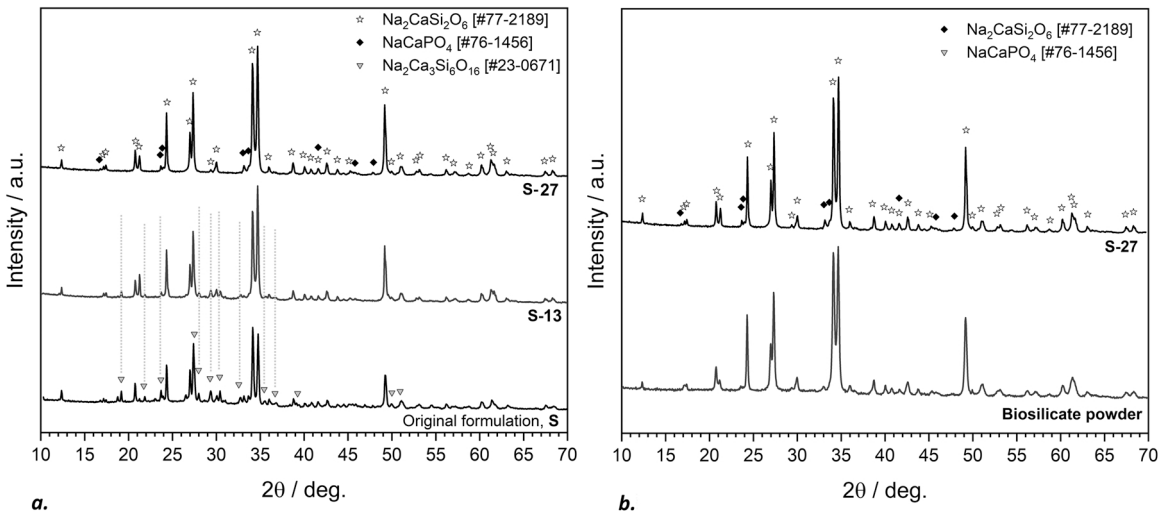

Fig. 3. a) Change of phase composition by reduction of silicone content; b) comparison with Biosilicate® glass-ceramic powder.

reduction, but disappeared completely with the 27% reduction. As shown in Fig. 3b, the diffraction pattern of the ceramic obtained from the mixture with the silicone content reduced by 27% resembled that of real Biosilicate® glass-ceramic powders.

The formation of the 'theoretical' silicate, despite the reduction of the amount of silicone, was attributed to deviations from the expected reaction path, assessed by chemical analysis. Both the powdered polymer-derived ceramics and Biosilicate® glass-ceramic powders prepared by the crystallization of a parent glass, recently used for other additive manufacturing studies [30] and used as a benchmark, were examined by energy dispersive X-ray spectroscopy (EDS). Powders homogenously distributed on a carbon tape, covering three areas of approximately 750 μm × 600 μm were analyzed.

With the ceramic residue reacting only partially to form Biosilicate-like material, some Si atoms in the polymer-derived (PD) material are expected to be included in SiC. The Na/Si and Ca/Si atomic ratios are consequently lower than those in Biosilicate® glass-ceramic, as follows:

$$(Na/Si) = \frac{Na}{Si_{in\ Biosilicate} + Si_{in\ SiC}} <$$

$$< (Na/Si)_{in\ Biosilicate} = \frac{Na}{Si_{in\ Biosilicate}}$$

$$(Ca/Si) = \frac{Ca}{Si_{in\ Biosilicate} + Si_{in\ SiC}} <$$

$$< (Ca/Si)_{in\ Biosilicate} = \frac{Ca}{Si_{in\ Biosilicate}}$$

The graph in Fig. 4 refers to normalized Na/Si and Ca/Si atomic ratios obtained from the experimental data, defined as:

$$\left(\frac{Na}{Si}\right)_{norm} = \frac{(Na/Si)_{exp\ in\ PD-material}}{(Na/Si)_{exp\ in\ Biosilicate}}$$

$$\left(\frac{Ca}{Si}\right)_{norm} = \frac{(Ca/Si)_{exp\ in\ PD-material}}{(Ca/Si)_{exp\ in\ Biosilicate}}$$

With 0.7 Si atoms in SiC for any 2.3 Si atoms bound in SiO_2, the normalized ratios $(Na/Si)_{norm}$ and $(Ca/Si)_{norm}$ would be equal to 2.3/(2.3 + 0.7) = 2.3/3 = 0.77. This ratio was confirmed for the product of the composition S, although it contradicted the formation of a relatively silica rich phase $Na_2Ca_3Si_6O_{16}$. On the contrary, for the product of S-27 formulation, the ratios practically matched those found in Biosilicate® glass-ceramic, being close to 1.

We can thus assume that a silicone-based blend of particular composition maintains, under all conditions, the expected yield of Si atoms in the final product; the deviations are related to preferential

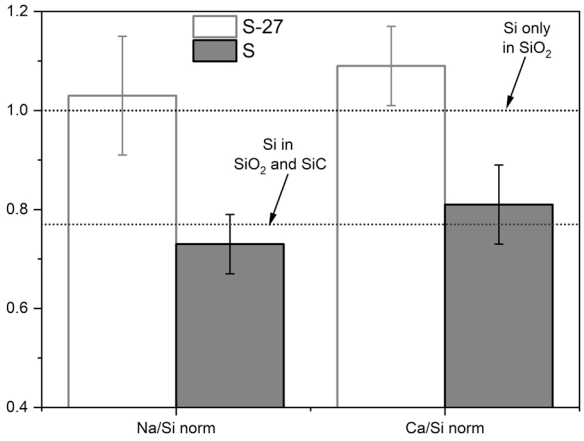

Fig. 4. Na/Si and Ca/Si ratios in polymer-derived materials, normalized with respect to the analogous ratios in a Biosilicate® glass-ceramic powder.

bonding of silicon with oxygen. In other words, the $Si_3O_{4.6}C_{8.45}$ ceramic residue likely decomposed to a simple mixture of pyrolytic carbon and silica, which reacted with Na_2O and CaO from the fillers.

The optimization of the phase assemblage of the product could be coupled with the control of overall porosity, using a gyroid scaffold model, shown in Fig. 2. This geometrical model is known to optimize the strength-to-density ratio, also in the perspective of bone implants [26].

The correlation between porosity of geometrical models and porosity of final products is not straightforward in stereolithography 3D printing. A significant contribution is related to the nature of the studied material. For example, in sintered glass-ceramics, a remarkable coarsening may be caused by viscous flow; if uncontrolled, it may degrade completely the three-dimensional structure created by printing [13]. In general, however, some issues may arise even before sintering, during the printing step. The use of suspensions of ceramic powders negatively affects the printing resolution in comparison to homogeneous liquid feedstock (Fig. 5a). Solid particles scatter light [31], altering the curing depth. This can be corrected by adjusting the exposition times, but curing of photosensitive resin outside the theoretical projection area (defined by horizontal cross-sections of the models) cannot be excluded (Fig. 5b). This reduces the porosity, since an extension of the projected area corresponds to an extension of solid occupancy in a printed layer. In the present case, we effectively observed a substantial decrease of overall porosity in printed parts, as shown in Fig. 6, although not uniform for

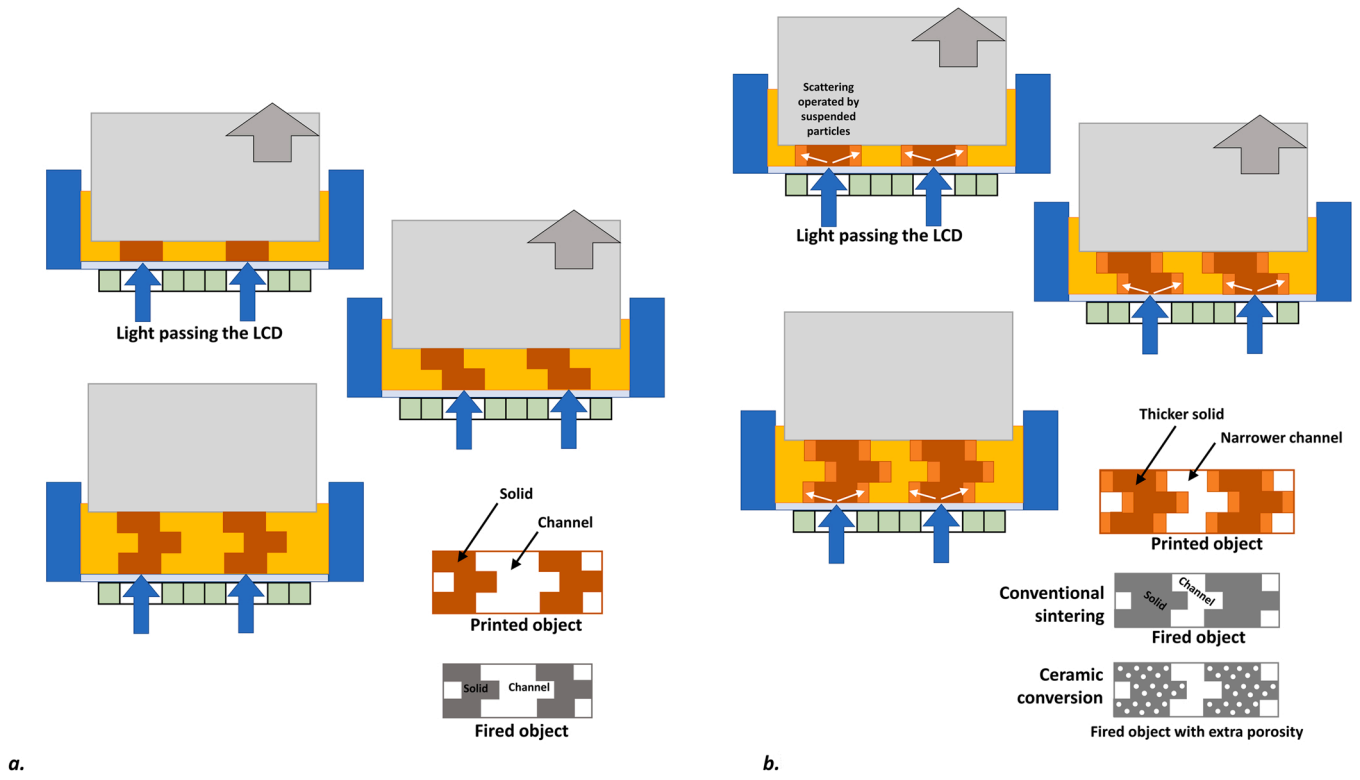

Fig. 5. a) Scheme of 'ideal' stereolithography; b) scheme of coarsening induced by light scattering.

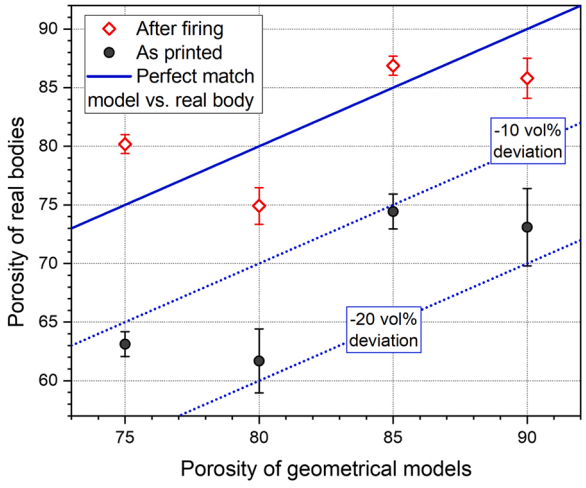

Fig. 6. Porosity of real bodies (after printing and after firing) compared to porosity of geometrical models.

different porosity values of reference models (from 11 to 18 vol%).

The thermal conversion of the silicone and the interaction between polymer-derived silica and filler actually counterbalanced the reduction of porosity due to scattering-induced coarsening. Cured parts were not intended to densify, as in conventional sintering, but they were expected to transform into porous walls (see bottom part of Fig. 5b) due to the gas release from fillers and the polymer matrix during the ceramic conversion. A limited amount of liquid phase (from sodium phosphate) and crystallization of $Na_2CaSi_2O_6$ prevented viscous flow. The overall porosity, almost completely open (according to He pycnometry), recovered a good match of sintered structures with the porosity of the models, as illustrated in Fig. 6. The fired scaffold based on a model with 85% porosity had a final overall porosity of ~87%, out of which ~85% was open. There was a homogeneous shrinkage, in all directions, of ~28%.

All fired samples were crack-free and homogenous, as illustrated by the optical microscope images in Fig. 7a,b (in real colors). SEM micrographs (Fig. 7c,d) revealed highly textured walls, expected to favor cell attachment, in good analogy with the microstructure of polymer-derived foams studied previously [24]. Similarly to the foams, higher magnification details (Fig. 7e,f) revealed the formation of fibrous bundles emerging from a microporous matrix. Such microstructure feature could promote the infiltration of body fluids into the scaffold. Such specific microstructure enhanced the specific surface area (SSA): while the SSA of Biosilicate glass-ceramic powders was 2.0 m^2/g, the SSA of coarser powders (sieved <70 μm) from crushed polymer-derived material was 71.2 m^2/g (based on the results of a test of powdered scaffold with 85% model porosity).

Excellent strength-to-density values were achieved for all polymer-derived Biosilicate materials, independently from their porosity. This observation is supported by the chart in Fig. 8, reporting an extensive comparison with highly porous materials from 'real' (=crystallized glass) Biosilicate® [30,32,33].

The chart displays the lines corresponding to the model proposed by Gibson and Ashby (GA) for a number of open-celled porous ceramics [34]. According to the model, under compression the open-celled bodies can be treated as lattices with structural elements represented by small beams, undergoing bending. For such lattices ('GA lattices'), the compressive strength (σ_c) is related to the bending strength (σ_{bend}) of the solid phase and the relative density (ρ_{rel}, defined as $\rho_{rel} = 1\text{-}P/100$, where P is the total porosity), following an exponential equation:

$$\sigma_c = C \cdot \sigma_{bend} \cdot \rho_{rel}^{3/2}$$

where C is a dimensionless constant (≈0.2). Each line plotted in the $1/\sigma_c$ vs ρ_{rel} chart corresponds to a specific value of σ_{bend}, from 50 to 250 MPa. The materials described by the points closer to the bottom left corner exhibit an excellent trade-off of high compressive strength and low density.

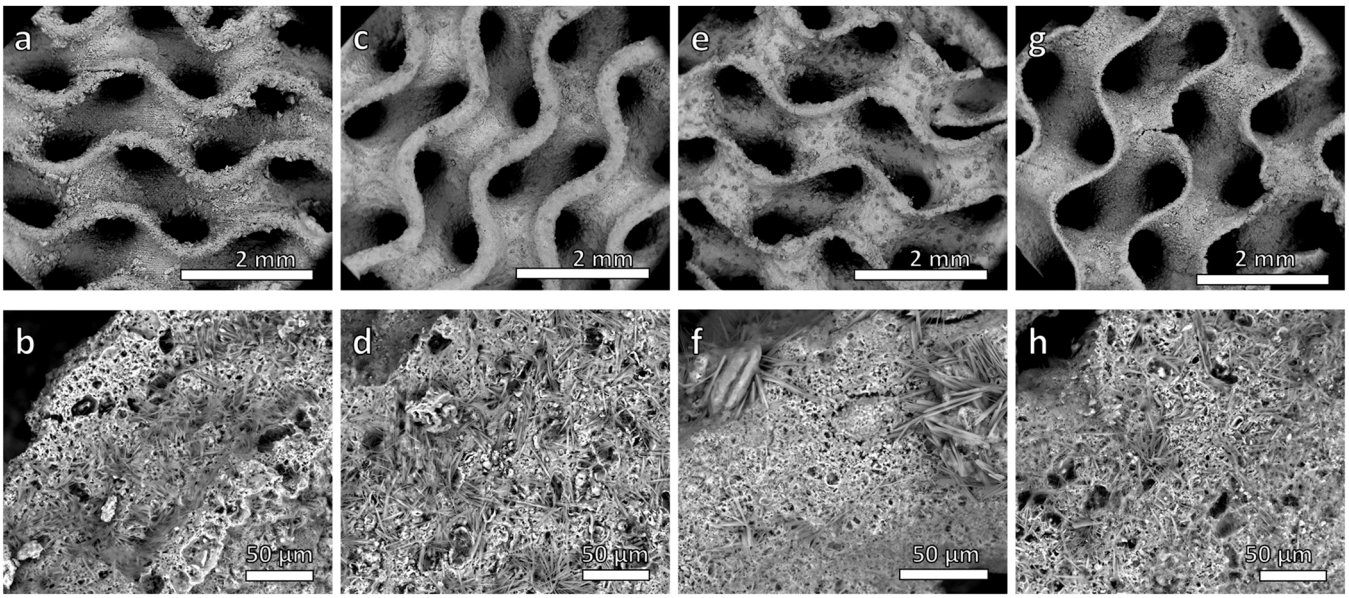

Fig. 7. Microstructural details of polymer-derived Biosilicate gyroid scaffolds: a,c,e) 80% model porosity; b,d,f) 85% model porosity.

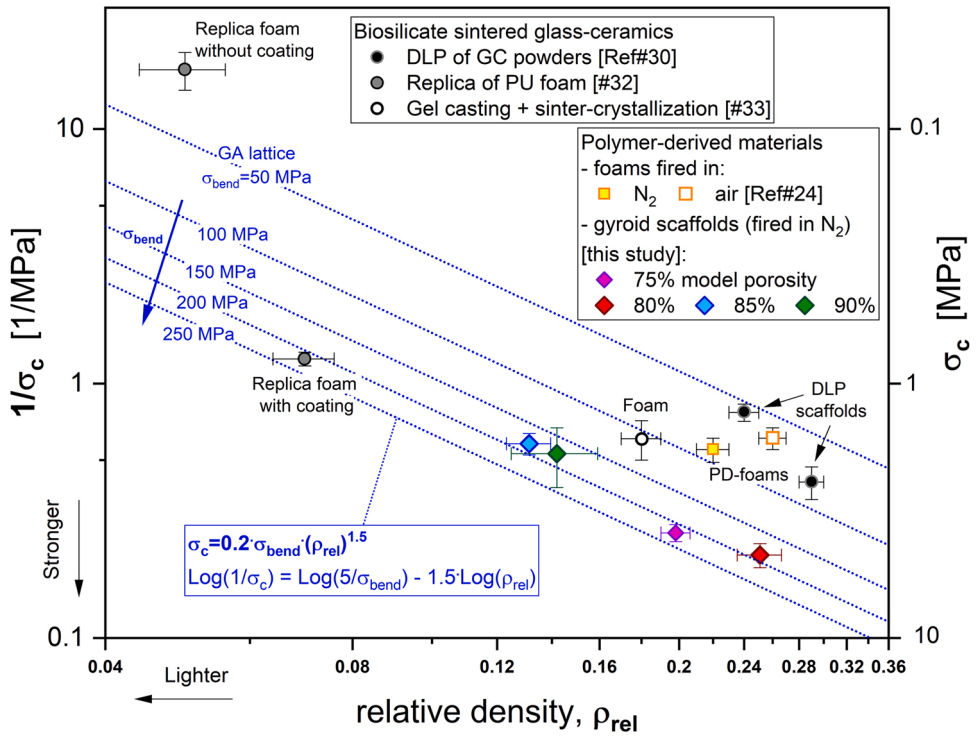

Fig. 8. Strength/relative density plot of developed porous materials compared to selected porous Biosilicate glass-ceramics from previously published data (polymer-derived (PD) foams from Dogrul et al. [24]; DLP scaffolds from Elsayed et al. [30], replica foams from Desimone et al. [32]; gel-casting foams from Bernardo et al. [33]).

Sintered Biosilicate® glass-ceramic foams fabricated by the replica technique by Desimone et al. [32], were highly porous (5% relative density, i.e. total porosity of 95%) but also quite weak (σ_c in the order of 0.06 MPa), being equivalent to GA lattices with σ_{bend} not exceeding 30 MPa. An improvement was achieved through the reinforcement of the solid phase by a gelatine coating, making the composite scaffolds equivalent to GA lattices with the σ_{bend} value of ~200 MPa. Such high values were not achieved by any other technology, that does not involve a coating step (e.g. DLP-printing and sintering, gel casting and sinter-crystallization [30,33]). Fig. 8, however, demonstrates that MSLA-processed polymer-derived gyroid scaffolds are equivalent to very strong GA lattices. They compare favorably also with Biosilicate-like polymer-derived foams prepared from the same H44 polymer and fired in air or nitrogen [9]. Stronger polymer-derived scaffolds may derive from direct ink writing (DIW), but with much lower overall porosity [14].

Biosilicate® glass-ceramics are a fundamental 'target' for the application of the technology of polymer-derived ceramics in the field of biomaterials. An extensive biological characterization of the developed composite scaffolds, involving cell culture studies, is undoubtedly

needed and it is the subject of current studies. Preliminary investigations on DIW-processed scaffold are promising [14]. The findings reported above are significant in the perspective of fabrication of implants with highly precise, tailored geometries, achievable only by stereolithography.

4. Conclusions

Masked stereolithography printing was successfully applied to polymer-derived materials resembling Biosilicate® glass-ceramics, starting from silicone/photocurable acrylates blends. The optimization of silicone/fillers ratio must support the adoption of the specific additive manufacturing technology, in order to achieve products matching the desired phase assemblage. The preparation of a glass-ceramic system from a polymeric precursor had an interesting interplay with the manufacturing technology, and the porosity formed during ceramic transformation of both the silicone precursor and the fillers compensated the deviations from target model porosity arising from printing operations.

Declaration of Competing Interest

The authors declare that they have no known competing financial interests or personal relationships that could have appeared to influence the work reported in this paper.

Acknowledgments

This paper is a part of the dissemination activities of the project FunGlass (Centre for Functional and Surface Functionalized Glass). This project has received funding from the European Union's Horizon 2020 research and innovation programme under grant agreement No. 739566. Discussions with Prof. A.R. Boccaccini (University of Erlangen-Nuremberg, Germany), scientific board member (Biomaterials) of the Centre for Functional and Surface Functionalized Glass, are greatly appreciated.

References

[1] A. Francis, R. Detsch, A.R. Boccaccini, Fabrication and cytotoxicity assessment of novel polysiloxane/bioactive glass films for biomedical applications, Ceram. Int. 42 (2016) 15442–15448, https://doi.org/10.1016/j.ceramint.2016.06.195.
[2] F. Xie, I. Gonzalo-Juan, H. Breitzke, C. Fasel, M. Trapp, G. Buntkowsky, H. J. Kleebe, R. Riedel, A.R. Boccaccini, E. Ionescu, Effect of Ca and B incorporation into silicon oxycarbide on its microstructure and phase composition, J. Am. Ceram. Soc. 102 (2019) 7645–7655, https://doi.org/10.1111/jace.16620.
[3] F. Xie, E. Ionescu, M. Arango-Ospina, R. Riedel, A.R. Boccaccini, I. Gonzalo-Juan, Facile preparative access to bioactive silicon oxycarbides with tunable porosity, Materials 12 (2019) 3862, https://doi.org/10.3390/ma12233862.
[4] M. Arango-Ospina, F. Xie, I. Gonzalo-Juan, R. Riedel, E. Ionescu, A.R. Boccaccini, Review: silicon oxycarbide based materials for biomedical applications, Appl. Mater. Today 18 (2020) 18, https://doi.org/10.1016/j.apmt.2019.100482.
[5] I. Gonzalo-Juan, F. Xie, M. Becker, D.U. Tulyaganov, E. Ionescu, S. Lauterbach, F. De Angelis Rigotti, A. Fischer, R. Riedel, Synthesis of silver modified bioactive glassy materials with antibacterial properties via facile and low-temperature route, Materials 13 (2020) 5115, https://doi.org/10.3390/ma13225115.
[6] A. Francis, Biological evaluation of preceramic organosilicon polymers for various healthcare and biomedical engineering applications: a review, J. Biomed. Mater. Res. 109 (2020) 744–764, https://doi.org/10.1002/jbm.b.34740.
[7] E. Bernardo, L. Fiocco, G. Parcianello, E. Storti, P. Colombo, Advanced ceramics from preceramic polymers modified at the nano-scale: a review, Materials 7 (2014) 1927–1956, https://doi.org/10.3390/ma7031927.
[8] A. Dasan, H. Elsayed, J. Kraxner, D. Galusek, E. Bernardo, Hierarchically porous 3D-printed akermanite scaffolds from silicones and engineered fillers, J. Eur. Ceram. Soc. 34 (2019) 4445–4449, https://doi.org/10.1016/j.jeurceramsoc.2019.06.021.
[9] H. Elsayed, P. Rebesan, M.C. Crovace, E.D. Zanotto, E. Bernardo, Biosilicate® scaffolds produced by 3D-printing and direct foaming using preceramic polymers, J. Am. Ceram. Soc. 102 (2018) 1010–1020, https://doi.org/10.1111/jace.15948.
[10] E. Zanchetta, M. Cattaldo, G. Franchin, M. Schwentenwein, J. Homa, G. Brusatin, P. Colombo, Stereolithography of SiOC ceramic microcomponents, Adv. Mater. 28 (2016) 370–376.
[11] J. Schmidt, P. Colombo, Digital light processing of ceramic components from polysiloxanes, J. Eur. Ceram. Soc. 38 (2018) 57–66.
[12] A. Dasan, H. Elsayed, J. Kraxner, P. Colombo, E. Bernardo, Engineering of silicone-based mixtures for the digital light processing of akermanite scaffolds, J. Eur. Ceram. Soc. 40 (2020) 2566–2572, https://doi.org/10.1016/j.jeurceramsoc.2019.11.087.
[13] H. Elsayed, M. Picicco, A. Dasan, J. Kraxner, D. Galusek, E. Bernardo, Glass powders and reactive silicone binder: application to digital light processing of bioactive glass-ceramic scaffolds, Ceram. Int. 46 (2020) 25299–25305, https://doi.org/10.1016/j.ceramint.2020.06.323.
[14] F. Dogrul, P. Ożóg, M. Michálek, H. Elsayed, D. Galusek, L. Liverani, A. R. Boccaccini, E. Bernardo, Polymer-derived Biosilicate®-like glass-ceramics: engineering of formulations and additive manufacturing of three-dimensional scaffolds, Materials 14 (2021) 5170, https://doi.org/10.3390/ma14185170.
[15] A. Saha, R. Raj, D.L. Williamson, A model for the nanodomains in polymer-derived SiCO, J. Am. Ceram. Soc. 89 (2006) 2188–2195, https://doi.org/10.1111/j.1551-2916.2006.00920.x.
[16] S. Fu, H. Hu, J. Chen, Y. Zhu, S. Zhao, Silicone resin derived larnite/c scaffolds via 3D printing for potential tumor therapy and bone regeneration, Chem. Eng. J. (2019), 122928, https://doi.org/10.1016/j.cej.2019.122928.
[17] T. Zhu, M. Zhu, Y. Zhu, Fabrication of forsterite scaffolds with photothermal-induced antibacterial activity by 3D printing and polymer-derived ceramics strategy, Ceram. Int. 46 (2020) 13607–13614, https://doi.org/10.1016/j.ceramint.2020.02.146.
[18] D. Shao, M. Lu, D. Xu, X. Zheng, Y. Pan, Y. Song, J. Xu, M. Li, M. Zhang, J. Li, G. Chi, L. Chen, B. Yang, Carbon dots for tracking and promoting theosteogenic differentiation of mesenchymal stemcells, Biomater. Sci. 5 (2017) 1820–1827, https://doi.org/10.1039/C7BM00358G.
[19] N. Saito, Y. Usui, K. Aoki, N. Narita, M. Shimizu, K. Hara, N. Ogiwara, K. Nakamura, N. Ishigaki, H. Kato, S. Taruta, M. Endo, Carbon nanotubes: biomaterial applications, Chem. Soc. Rev. 38 (2009) 1897–1903.
[20] Ogihara, Usui, Aoki, et al., Biocompatibility and bone tissue compatibility of alumina ceramics reinforced with carbon nanotubes, Nanomedicine 7 (2012) 981–993, https://doi.org/10.2217/nnm.12.1.
[21] S. Shafiei, M. Omidi, F. Nasehi, H. Golzar, D. Mohammadrezaei, M.R. Rad, A. Khojasteh, Egg shell-derived calcium phosphate/carbon dot nanofibrous scaffolds for bone tissue engineering: fabrication and characterization, Mater. Sci. Eng. C 100 (2019) 564–575, https://doi.org/10.1016/j.msec.2019.03.003.
[22] C. Wu, L. Xia, P. Han, M. Xu, B. Fang, J. Wang, J. Chang, Y. Xiao, Graphene-oxide-modified β-tricalcium phosphate bioceramics stimulate in vitro and in vivo osteogenesis, Carbon 93 (2015) 116–129, https://doi.org/10.1016/j.carbon.2015.04.048.
[23] C. Gao, P. Feng, S. Peng, C. Shuai, Carbon nanotube, graphene and boron nitride nanotube reinforced bioactive ceramics for bone repair, Acta Biomater. 62 (2017) 1–20, https://doi.org/10.1016/j.actbio.2017.05.020.
[24] F. Dogrul, S. Bortolin, D. Del Col, N. Dengo, D. Pedron, M. Michalek, H. Elsayed, D. Galusek, E. Bernardo, Polymer-derived Biosilicate-C composite foams: phase development and photothermal effect, J. Eur. Ceram. Soc. 41 (2021) 380–388, https://doi.org/10.1016/j.jeurceramsoc.2021.09.012.
[25] C.-P. Jang, T. Meizinta, Development of LCD-based additive manufacturing system for biomedical application, in: ICAIR-CACRE '16: Proceedings of the International Conference on Artificial Intelligence and Robotics and the International Conference on Automation, Control and Robotics Engineering (2016) 1–6. DOI: https://doi.org/10.1145/2952744.2952764.
[26] A. Aut Yánez, A. Herrera, O. Martel, D. Monopoli, H. Afonso, Compressive behaviour of gyroid lattice structures for human cancellous bone implant applications, Mater. Sci. Eng. C 68 (2016) 445–448.
[27] G. Savio, R. Meneghello, G. Concheri, Design of variable thickness triply periodic surfaces for additive manufacturing, Prog. Addit. Manuf. 4 (2019) 281–290.
[28] S. Rosso, A. Curtarello, F. Basana, L. Grigolato, R. Meneghello, G. Concheri, G. Savio, Modeling symmetric minimal surfaces by mesh subdivision, in: L. Roucoules, M. Paredes, B. Eynard, P. Morer Camo, C. Rizzi (Eds.), Advances on Mechanics, Design Engineering and Manufacturing III. JCM 2020. Lecture Notes in Mechanical Engineering, Springer, Cham, 2020, pp. 249–254.
[29] M. Scheffler, T. Takahashi, J. Kaschta, H. Muensted, P. Buhler, P. Greil, Pyrolytic decomposition of preceramic organo polysiloxanes. Innovative Processing and Synthesis of Ceramics, Glasses, and Composites IV: Ceramic Transactions, 2000, pp. 239–250.
[30] H. Elsayed, P. Colombo, M.C. Crovace, E.D. Zanotto, E. Bernardo, Suitability of Biosilicate® glass-ceramic powder for additive manufacturing of highly porous scaffolds, Ceram. Int. 47 (2021) 8200–8207, https://doi.org/10.1016/j.ceramint.2020.11.179.
[31] C. Qian, K. Hu, J. Li, P. Li, Z. Lu, The effect of light scattering in stereolithography ceramic manufacturing, J. Eur. Ceram. Soc. 41 (2021) 7141–7154, https://doi.org/10.1016/j.jeurceramsoc.2021.07.017.
[32] D. Desimone, W. Li, J.A. Roether, D.W. Schubert, M.C. Crovace, A.C.M. Rodrigues, E.D. Zanotto, A.R. Boccaccini, Biosilicate®—gelatine bone scaffolds by the foam replica technique: development and characterization, Sci. Technol. Adv. Mater. 14 (2013), 045008.
[33] E. Bernardo, H. Elsayed Hamada, A. Rincon Romero, M.C. Crovace, E.D. Zanotto, T. Fey Tobias, Biosilicate® glass-ceramic foams from refined alkali activation and gel casting, Front. Mater. 7 (2021), 588789, https://doi.org/10.3389/fmats.2020.588789.
[34] L.J. Gibson, M.F. Ashby, Cellular Solids: Structure and Properties, Cambridge Pniversity Press, Cambridge, UK, 1999.